frontiers | Frontiers in Built Environment

ORIGINAL RESEARCH
published: 23 May 2022
doi: 10.3389/fbuil.2022.840159

Traditional Structures in Turkey and Greece in 30 October 2020 Aegean Sea Earthquake: Field Observations and Empirical Fragility Assessment

Yasemin D Aktas[1], Ioanna Ioannou[1], Fatma Sevil Malcioglu[2], Ahsana Parammal Vatteri[1], Maria Kontoe[1], Kokcan Donmez[2], Jacob Black[3], Danai Kazantzidou-Firtinidou[4], Panagiotis Dermanis[5] and Filiz Diri-Akyildiz[1,6]*

[1]Epicentre Research Group, Department of Civil, Environmental and Geomatic Engineering, University College London (UCL), London, United Kingdom, [2]Department of Earthquake Engineering, Bogazici University, Istanbul, Turkey, [3]Civil and Environmental Engineering Department, Imperial College London, London, United Kingdom, [4]Seismological Laboratory, Faculty of Geology and Geoenvironment, National Kapodistrian University of Athens, Athens, Greece, [5]Department of Civil Engineering, University of Patras, Patras, Greece, [6]Cultural Heritage Conservation Programme, Faculty of Architecture, Middle East Technical University, Ankara, Turkey

OPEN ACCESS

Edited by:
Hugo Rodrigues,
University of Aveiro, Portugal

Reviewed by:
Leonidas Kouris,
Aristotle University of Thessaloniki, Greece
Maria Teresa De Risi,
University of Naples Federico II, Italy

***Correspondence:**
Yasemin D Aktas
y.aktas@ucl.ac.uk

Specialty section:
This article was submitted to Earthquake Engineering, a section of the journal Frontiers in Built Environment

Received: 20 December 2021
Accepted: 30 March 2022
Published: 23 May 2022

Citation:
Aktas YD, Ioannou I, Malcioglu FS, Vatteri AP, Kontoe M, Donmez K, Black J, Kazantzidou-Firtinidou D, Dermanis P and Diri-Akyildiz F (2022) Traditional Structures in Turkey and Greece in 30 October 2020 Aegean Sea Earthquake: Field Observations and Empirical Fragility Assessment. Front. Built Environ. 8:840159. doi: 10.3389/fbuil.2022.840159

On 30th October 2020, an earthquake of magnitude 6.9 hit the Aegean coasts of Turkey and Greece. The epicentre was some 14 km northeast of Avlakia settlement on Samos Island, and 25 km southwest of Turkish town Seferihisar, Izmir. The destruction the earthquake caused concentrated mainly on the mid-rise RC buildings in certain districts of Izmir city. Among the diverse building typologies affected by the event are the traditional/vernacular hybrid timber-masonry and masonry buildings that are common to Turkey and Greece. This paper summarises and discusses the damage levels and mechanisms observed in these types of buildings, based on an extensive field and remote reconnaissance survey in the affected areas in both countries conducted by the Earthquake Engineering Field Investigation Team (EEFIT) of the United Kingdom Institute of Structural Engineers (IStructE). The observed damage is then discussed in light of the level of maintenance and occupancy status. The collected data are also used to empirically construct fragility curves, to assess whether a small sample can be used to describe the overall performance of the buildings in the area and how these compare to the outcomes of previous studies on comparable building stocks.

Keywords: Aegean Earthquake, timber, masonry, fragility, vernacular, traditional

1 INTRODUCTION

Both Turkey and Greece are part of the seismically prone Mediterranean basin, and are frequently exposed to destructive earthquakes. The 30thOctober 2020 Aegean Earthquake of M_w = 6.9 was one of these—the largest peak ground acceleration (PGA) acquired in the closest station in the east of Samos Island was 0.24 g. However, the Samos possessed only two strong ground motion recordings and suffered from the lack of ground motion data, making a comprehensive assessment of the entire island difficult. Also, these two ground motions produced spectral accelerations larger than those of the design spectra of EAK (2003) and EC8 seismic provisions at approximately 0.5 s of the period. The Turkish side rattled with slightly lower peak ground accelerations than Samos but similarly,

spectral accelerations of the closest station excessed the design spectra of 1975, 2007, and 2018 Turkish seismic codes at 0.5 s and also 0.2 s of periods. On the other hand, all spectral accelerations of recorded ground motions in İzmir Basin, in which exposed to severe damage, were smaller than those of elastic design spectra (Malcioglu et al., 2022).

The 30th October 2020 Aegean Earthquake resulted in more than 120 fatalities, mainly due to the collapse of a very small number of mid-to high-rise RC buildings in two districts in Izmir, Turkey. Nonetheless, the affected area includes a wide variety of building typologies in addition to reinforced concrete. This study concentrates on the seismic performance of the traditional/vernacular buildings, both masonry and timber-masonry, which are well represented in the building inventory of the affected area. The seismic performance of these structures is examined here from the data collected during the EEFIT's hybrid reconnaissance mission in the aftermath of the 30th October Aegean Earthquake. As the event took place during the global COVID-19 pandemic, the mission combined remote and conventional field investigation techniques: while the local field crews visited some targeted areas to collect data on the building and damage characteristics, the rest of the team has remotely scanned through diverse sources (e.g., official damage data, local press and social media) to identify comprehensive (and ideally geotagged) visual material which can be used to better understand the impact of the event in the affected area (see Aktas et al., 2021; Aktas et al., 2022 for the mission setup and alternative data sources exploited for remote building damage assessment). Overall, a total of 304 traditional buildings have been surveyed, in the field and remotely, 90% of which are located in Samos including masonry (75%) and hybrid timber-masonry buildings (25%) in Samos city, Vathy, Kokkari, Karlovasi and Kontaiika in the Island of Samos, and Izmir city and Seferihisar in Turkey. The buildings were mostly used as dwellings, but commercial and mixed (i.e., residential and commercial) use were also observed. Although most buildings were in use, a notable 14% of the surveyed buildings were abandoned with visible signs of decay. The relatively large number of abandoned buildings found during the survey is consistent with the systematic decline of the population in Samos since the 1950s (EL.STAT, 2011).

In what follows, general information regarding the two traditional building typologies of the Aegean region are presented and their seismic performance during the 30th October 2020 earthquake is discussed based on the post-disaster observations collected during EEFIT's reconnaissance mission. The damage data produced based on the European Microseismic Scale (EMS-98) are then used to empirically construct fragility curves. These curves are, finally, compared to existing empirical fragility curves for similar buildings in the area to assess whether this small sample can be used to reliably quantify the likelihood of damage of the traditional buildings in the area and an overall discussion of the results follows.

A general description of each of these two typologies, common damage mechanisms under earthquake loading and their performance in 30 October event are discussed in the subsequent sections.

2 TRADITIONAL BUILDING STOCKS IN THE AFFECTED AREAS AND OBSERVATIONS FOLLOWING 30 OCTOBER 2020 EVENT

2.1 Timber-Masonry Structures

The timber-masonry structures are characterised by hybrid or "dual" construction system, composed of a masonry ground floor and timber frame upper floors (**Figure 1A**), with infill or cladding (**Figure 1B,C**, respectively). In certain cases, a masonry service wall with the chimney may carry on in the upper floors. The overall construction characteristics and structural principles of this hybrid typology which is common in Turkey, Greece and the Balkans, definitely since early 16th century if not earlier, are pretty well established, with however very rich variations in detailing, material selection and implementation from region to region (see Sahin-Guchan, 2018 for a systematic review of typologies based in Turkey; see (Dutu et al., 2018) for the Romanian examples (Papaioannou, 1961); specifically for Samos). They are often 2-3 storey buildings, where the construction materials and details of both the masonry ground floor and the braced timber frame upper floors can be extremely diverse: brick, stone, brick + stone or adobe masonry with or without tie-beams and/or timber posts at the ground floor are coupled with timber frames with brick, stone, brick + stone, adobe or timber infill or cladding. In the infilled typologies, the masonry infill is confined in small compartments created within the timber framing through diagonals and secondary members, to minimise the shear failure and maximise energy dissipation (**Figure 1D**; Aktas et al., 2014). Timber frames are occasionally accompanied by an additional external layer of masonry (**Figure 1E,F**). In the cladded typologies, mostly 3–4 cm wide laths are nailed onto the inner and outer surfaces of the timber frame, creating a very lightweight structure with a good diaphragm action. The connections are almost exclusively made of nails, which improve energy dissipation under seismic loading for enhanced ductility–the carpentry joints are existent, but are rare and simple. Metal connectors between masonry and timber floors are a reginal variation intrinsic to Lefkas (Vintzileou et al., 2007). Jetties (projections) are an optional but dominant feature of these houses, which can be built simply in the form of a cantilever or can be braced (Aktas, 2017). These are often used to have a better street view (**Figure 1G**) and occasionally also to "correct" the irregular ground floor plan (**Figure 1H**).

2.1.1 Timber-Masonry Structures: Common Damage Mechanisms

The common damage mechanisms of hybrid timber-masonry structures were identified as damage to the masonry ground floor, which triggers partial or global collapse, and out-of-plane failure of service walls or masonry infill. Two events that exemplify these are the Mw = 7.1 Gediz Earthquake in 1970, where the damage was attributed to the poor-quality masonry made of local stone and mudbrick/mud mortar, and the round timber posts (Mitchell 1976; Şahin-Güçhan, 2018) and the Mw = 6.3 Lesvos Earthquake in 2017, where the poor-quality material and poor workmanship were deemed the main reasons behind damage

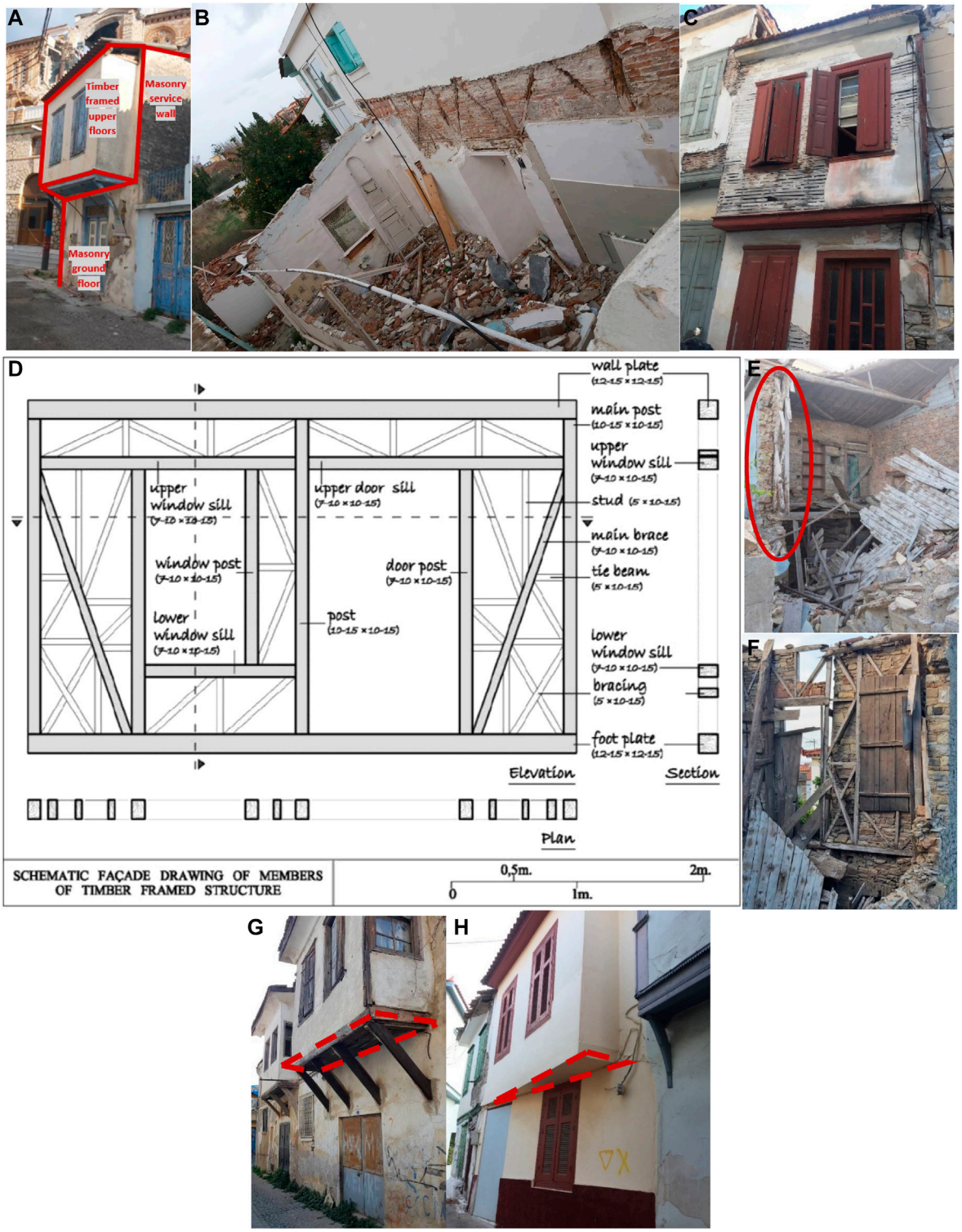

FIGURE 1 | (A) General construction features of hybrid timber-masonry structures (in Samos, Greece) with examples to **(B)** infilled and **(C)** cladded typologies (in Samos, Greece); **(D)** The schematic showing the general timber frame organization based on a Western Anatolian case, Turkey (Diri, 2010) **(E,F)** Examples of timber framed walls with an additional external layer of masonry (in Samos, Greece); **(G)** a regular braced jetty (in Seferihisar, Turkey); **(H)** an irregular cantilever jetty (in Samos, Greece).

FIGURE 2 | Examples of timber-masonry structures which suffered from failure of masonry: **(A–C)** out of plane infill failure of masonry in the upper floors, **(D,E)** failure of masonry ground floor and timber frames above **(F)** total collapse induced by the failure of the masonry ground floor [**(B,E)** from Mikres Diadromes Samou, 2020] [DG3-DG5] (all in Samos, Greece).

(Gocer, 2020). Heavy deterioration in timber or at the connections were found responsible of the damage observed in timber-framed structures at the Mw = 6 Orta Earthquake in 2000 (Demirtaş et al., 2000; Gulkan and Langenbach 2004; Langenbach 2007) and at the Mw = 7.1 Mudurnu Earthquake in 1967 (Ambraseys and Jackson, 1981; Spence 2014). We learn from Ambraseys and Zatopek (1969) also that the structures with large ground floor openings were also exclusively damaged in this latter event–a phenomenon observed to have caused damage at the Gediz Earthquake too (Sahin-Guchan, 2018). One of the factors critical to ensuring a good performance under seismic action is good connection between different structural components throughout. The lack of such good connections due to either poor construction practices or age caused total collapses following the Mw = 6.2 2002 Afyon, Sultandağı (Çay) Earthquake (Erdik et al., 2002) and the Mw = 6.4 2003 Bingol Earthquake (Erdik et al., 2003). Other significant events that evidenced good performance include the Mw = 6.1 1992 Erzincan Earthquake, where the impact of the earthquake on these buildings was limited to cracking of plaster, or to minimal lateral deflections while still standing (Erdik et al., 1992; Williams et al., 1992), 1995 Dinar Earthquake (Biricik et al., 1996), and 1999 Marmara earthquakes (Tobriner 2000; Gülhan and Özyörük Güney, 2000).

2.1.2 Timber-Masonry Structures: Performance in 30 October Aegean Sea Earthquake

During the 2020 EEFIT's Aegean mission, 76 hybrid timber-masonry buildings were surveyed in the field and remotely (see Aktas et al., 2022). The vast majority of buildings were 2-storey high (>95%) and aged constructions. On both the Samos and Turkish coasts, the main material for the masonry ground floor is stone. There is a good mix of infilled and cladded typologies (although there is also a substantial portion of buildings where the materials cannot be identified due to plaster). In a few examples in Samos, the cladding is also present in the ground floor façade. Of the surveyed buildings, 61% were found to have at least one type of irregularity, with the jetty on one of the façades being the most prominent one. Moreover, 58% were attached to an adjacent building increasing their pounding potential. Overall, the surveyed buildings were found to be in a poor state of conservation with 27% being abandoned. Of the buildings still in use 28% had visible signs of damage from before the 30th October seismic event.

Around half of the hybrid timber-masonry traditional structures performed well in the recent earthquake, evidenced by the many structures withstanding the event without any visible damage or minor non-structural damage, such as cracking or falling of plaster. However, some moderate or heavy structural damage cases were also observed as described in the subsequent sections.

2.1.2.1 Damage to/Initiated by Masonry

One of the most common damage mechanisms, observed in the 2020 Aegean Earthquake as well as the previous events is the out-of-plane failure of masonry. This may impact masonry infill within timber frames on the upper floors (**Figure 2A,B**), masonry the service wall (**Figure 2C**), or masonry ground floor ((**Figures 2D–F**). This behaviour can be particularly exacerbated by the poor masonry material, such as the low-quality multi-leaf masonry

FIGURE 3 | Examples of damage to timber framing in timber-masonry structures. **(A and B)**: progressive failure of the upper floor timber framing and the roof [DG4-DG5]; **(C)** Overturning of the jetty in timber-masonry structures [picture on the left from Mikres Diadromes Samou, 2020] [DG3] (all in Samos, Greece).

shown in **Figure 2A**, where the colour suggests that a mud-based mortar was used. The failure of ground floor masonry material might trigger failure of an entire timber frame on top (**Figure 2D, E**) or may lead to progressive collapse (**Figure 2F**).

2.1.2.2 Damage to Timber Framing

Apart from the common cases of masonry failure discussed in the previous section, there are also those cases where the timber framing is damaged independently from the masonry failure, leading progressively to the roof collapse (**Figure 3A,B**). The weakened connections within and between the individual timber frames, and between the masonry ground floor and the timber framed upper stories are the common triggers for this type of damage. Sometimes damage may be concentrated at the cantilevered sections, i.e. jetties (**Figure 3C**).

2.2 Masonry Structures

The traditional masonry structures in the areas affected by the 30 October 2020 Aegean earthquake are almost exclusively made of stone, with however diverse unit, binder and

FIGURE 4 | Examples of the surveyed traditional masonry building stock: **(A)** Mostly cut stone masonry; **(B)** Masonry with irregular sizes of stone and brick, with tie beams shown in red; **(C)** Cut stone masonry structure with a pronounced elevation irregularity and corner strengthening, **(D)** Roughly cut stone masonry, **(E)** Shallow brick masonry arch lentil, **(F)** Masonry wall with roughly carved stones, slate and tie beams) (all in Samos, Greece); **(G)** Stone masonry structure in Turkey.

morphological features, and have a timber roof structure (**Figure 4**). Most commonly, these are made of roughly cut large stones and lime mortar, with thin slates or smaller pieces of stone, occasionally round pebbles, also inserted to fill in the gaps. There are cases where mud-mortar is observed, or the apparent multi-leaf masonry walls evident after the failure. Tie-beams are commonly used to strengthen the masonry. Additionally, the use of bricks in the lintels is quite common (**Figure 4E**). Traditional masonry structures in Turkey are almost exclusively plastered from outside, making it difficult to read the details of the construction system (**Figure 4G**). Around 17% of them is single storey and 70% is two storey. The most common irregularity we observe in >1 storey examples of these structures was the variation of floor heights, with the ground floor being higher. Change in stiffness due to structures attached to the main building is also common.

2.2.1 Masonry Structures: Common Damage Mechanisms

The structural performance of masonry under earthquake loading can be very diverse, and depend heavily on the quality of construction, the masonry units and the binder, the construction morphology, among others. Very commonly, however, damage mechanisms include in- and out-of-plane failure, overturning and corner failure, due for instance to lack or poor quality of connections, large openings, low mechanical properties of the masonry material or the assemblage, or plan irregularities. The most common damage patterns were identified as various out-of-plane mechanisms including overturning and corner damage and in-plane mechanisms manifesting mainly as shear cracks (see D'Ayala and Paganoni, 2011) for the damage description following the Mw = 6.3 L'Aquila earthquake in 2009, Vlachakis et al., 2020 following the Mw = 6.3 Lesvos Earthquake in 2017, and Karantoni and Bouckovalas, 1997 for the Mw = 5.5 Pyrgos Earthquake in 1993).

2.2.2 Masonry Structures: Performance in 30 October Aegean Sea Earthquake

During the mission, 228 masonry buildings were surveyed in the field as well as remotely (see Aktas et al., 2022 for alternative data sources). The overwhelming majority of these buildings were either one (almost 30%) or two storeys (>65%) and old stone masonry constructions. From the surveyed buildings, 14% were found to have at least one type of irregularity, primarily enlarged openings in the ground floor. Moreover, 38% of the building were

FIGURE 5 | Examples of out-of-plane failure in masonry structures: **(A)** Partial overturning of the external leaf; **(B)** Corner failure and partial overturning of gable; **(C)**: Out-of-plane failure of the external lead of a multi-leaf masonry wall with mud mortar; **(D)** Out-of-plane failure of a brick wall) [DG3-DG5](all in Samos, Greece).

attached to an adjacent building increasing their pounding potential. Similar to the hybrid timber-masonry buildings, a large percentage of the surveyed masonry buildings were found to be in a poor state of conservation with 11% being abandoned with visible damages due to decay, and around 24% of the buildings still in use but with pre-earthquake damage, including accumulated material degradation and structural decay. Lack of maintenance is particularly influential on timber components, i.e. roof and floor systems. Almost 40% of all surveyed buildings survived the event largely undamaged. There was no systematic damage pattern which suggests that there is a problem in the wall-to-wall, wall-to-roof and wall-to-floor connections. The damage mechanisms observed in the rest are discussed below.

2.2.2.1 Out-Of-Plane Failure

Out-of-plane masonry failure is one of the most common damage patterns we observe in the Aegean traditional masonry typologies following the 30 October Aegean Earthquake. It is evident in multiple ways: vertical or partial overturning, and corner failure are the most common types. Sometimes the overturning of the external leaf of the masonry walls is triggered by the in-plane failure of the façade (**Figure 5**). The extent of this type of failure is often limited to part of the façade however, and does not seem to be governed by its connection to the perpendicular walls. The interaction between the roof and the perimeter walls is a common cause of the out of plane failure at the higher elevations in a façade.

2.2.2.2 In-Plane Failure

In-plane failure is often characterised by shear or flexural cracking, a common damage mechanism in the masonry structured surveyed in this study, which manifests as cracking in the spandrels and diagonal cracking in the piers are very common. The strength of the lintels over the façade openings is an important determinant of the failure patterns in spandrels. Shear failure is observed mainly in case of weaker lintels (such as shallow masonry lintels), while flexural mode is more common for spandrels supported by strong lintels (**Figure 6**). How

FIGURE 6 | Examples of in-plane failure in masonry structures (all in Samos, Greece).

widespread the failure over the rest of the façade might be seen as an indicator of the homogeneity of the wall morphology.

2.3 Damage due to Pounding

Pounding refers to the lateral collision of abutting buildings during earthquakes, and it is a common cause of damage for building terraces under earthquake loading. Pounding induced damage manifests in the form of cracks along the interface between the adjoining buildings, and is commonly observed in both the terraced timber-masonry (**Figure 7** top row) and masonry buildings (**Figure 7** bottom row) in the areas affected by the 30 October 2020 event.

3 EMPIRICAL FRAGILITY ASSESSMENT

3.1 Main Characteristics of Vernacular Building Database and Strong Ground Motions

Having examined the seismic performance of the traditional/vernacular buildings during the 2020 Aegean earthquake, the data collected during the reconnaissance mission are used here to quantify the fragility of the traditional buildings in both countries. It should be noted that the fragility assessment is based only on the field data, as they have been systematically collected by the teams making sure that all the buildings of a selected street are surveyed without ignoring the undamaged buildings. This systematic approach, however, could not be followed for the remote damage assessments. Thus, the remotely assessed data are biased towards the damaged buildings and not suitable for the empirical assessment of buildings. Moreover, the abandoned buildings have been excluded from the analysis as it was not always possible to assess the extent of the seismic damage. For example, some abandoned buildings were missing their roof and it was not possible to establish whether this was caused by the earthquake. Overall, data from 140 traditional buildings (i.e., 77% are masonry and the remaining have dual-system of load bearing masonry and timber frame) are used for the analysis. The buildings are mostly used as dwellings but commercial or mixed use (i.e., commercial and residential) buildings are also included as their seismic performance is considered similar. See **Supplementary Material** (**Supplementary Figures S1, S2**) for details and the location of the buildings used for the empirical fragility assessment.

A considerable amount of strong ground motions of the 30.10.2020 Aegean Sea earthquake were recorded by the stations of four different networks namely the Ministry of

FIGURE 7 | Examples of pounding induced damage in timber-masonry structures [DG2-DG3] (Samos, Greece) Examples of pounding induced damage in timber-masonry structures [left picture from Mikres Diadromes Samou, 2020] [DG2-DG4] (all in Samos, Greece).

Interior Disaster and Emergency Management Presidency (AFAD), Boğaziçi University's Kandilli Observatory and Earthquake Research Institute (KOERI), National Observatory of Athens Seismic Network (HL) and ITSAK Strong Ground Motion (HI). The spatial distribution of the strong ground motion stations and the location of the inspected vernacular buildings used for the empirical fragility assessment considering their estimated damage grades are depicted in **Supplementary Figure S2**. Although the 80% of the inspected buildings are in the closest mainland to the epicentre, the Samos Island (Greece), there exist only two strong ground motion stations (SAMA and SMG1 in Vathy) that recorded the mainshock there. On the other hand, the Northwestern and North Central coasts (Karlovasi, Kontaiika and Kokkari) of Samos Island, in which the majority of the buildings with damage grades (DGs) larger than three are concentrated, suffer from the lack of ground motion recordings. The higher damage levels of these buildings may be associated with the close proximity of these settlements to the epicentre (10–15 km) and the Samos Basin fault. However, the absence of ground motion data makes it impossible to conduct a meaningful relation between damage levels and ground motion features for these places. The strong ground motion stations are much well-spread in the Turkish territory; nonetheless, the damage grades of all inspected vernacular buildings (20% of the regarded building database) in Seferihisar and the South of the İzmir Gulf are less than DG2.

The evaluation of ground motion levels together with soil conditions may provide meaningful indications to fathom the main determinants of the building damages. In **Figure 8**, the map shows the spatial distribution of the USGS topography-based V_{S30} (average shear wave velocities for the upper 30 m depth) (Allen and Wald, 2007) values for the sake of the integrity of the assessment. Additionally, the histogram in **Figure 8** showcases the distribution of V_{S30} values of soils under all inspected buildings. It is difficult to ascertain whether the building damage grades are directly dependent on the soil conditions. Herein, outdated seismic provision is taken into account in the evaluations since the inspected buildings were traditionally constructed. The majority of the V_{S30} values falls into soil class II based on the soil classification proposed by the 1975 Turkish Seismic Code. It is also worth noting here that B and Γ type of soils in EAK 2003 (Greek seismic code) covers 180–360 m/s according to (Pitilakis et al., 2004).

Furthermore, two horizontal components (East-West (EW) and North-South (NS)) of the recorded strong ground motions closest to the examined buildings are particularly assessed in **Figure 8** in terms of both PGAs and also spectral accelerations (SAs). The labeled stations in **Supplementary Figure S2** have been chosen based on criteria that the distance between the station and the closest inspected building should be less than about 2 km. Additionally, the closest station (GMLD) to the epicentre on the Turkish side is also added to the figure due

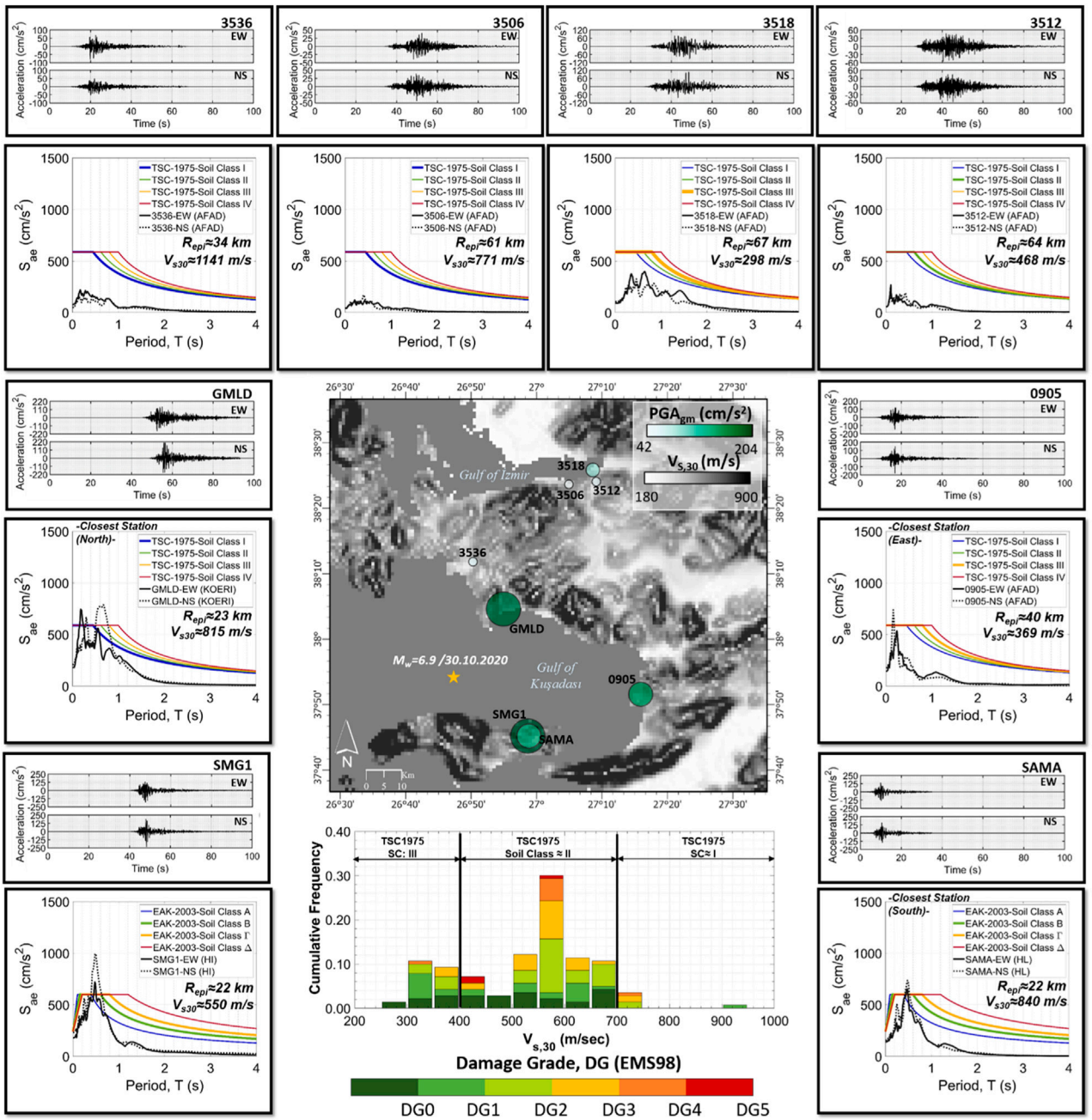

FIGURE 8 | The map of USGS topography based V_{S30} values together with the geometrical mean of recorded PGAs of several stations that are close to the examined buildings in the database, their strong ground motion time histories of horizontal components and their response spectra (5% of damping ratio) compared to design spectra (EAK2003 for Greece and Turkish seismic provision, 1975 for Turkey). The histogram shows the distribution of V_{S30} values of the inspected buildings with respect to their damage grades. (PGA_{gm} = Geometrical mean of peak ground acceletation; V_{S30} = average shear wave velocities for the upper 30 m depth; R_{epi} = Epicentral distance).

to its proximity to the epicentre although any inspected building located around GMLD does not consist in the building database of this study.

The geometrical mean of recorded PGAs designated on the map reveals that the closest station, SMG1, have been produced the highest PGA (PGA_{SMG1}≈204 cm/s^2). The PGA recorded in station SAMA, which is roughly at the same epicentral distance as SMG1, is lower than the PGA of the latter. This lower PGA in SAMA may be associated with the fact that SAMA has been deployed on the stiffer soil ($V_{S30,SAMA}$≈ 840 m/s). Moreover, there exist several buildings, whose damage grades are higher than DG2, around SMG1 while the damage grade of all

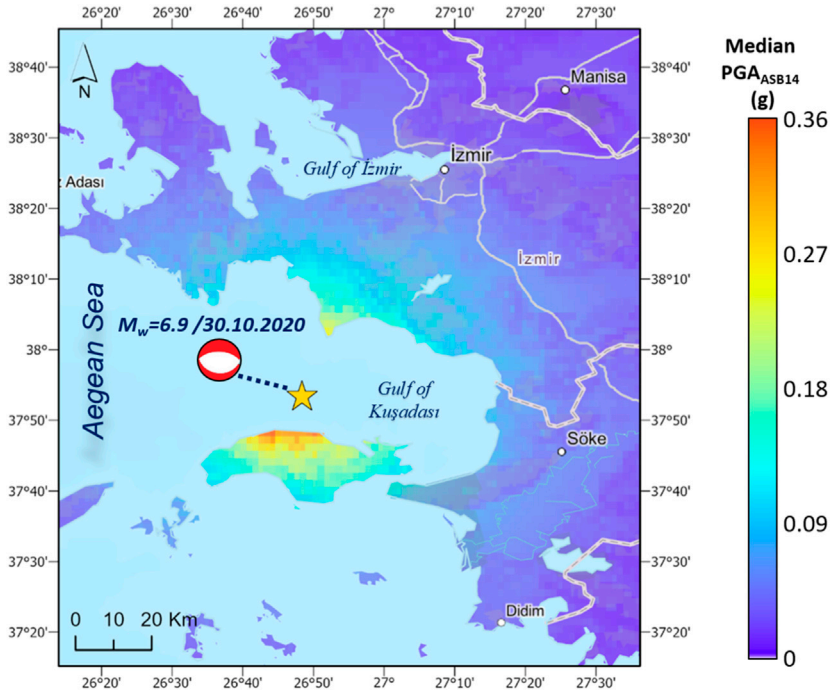

FIGURE 9 | The spatial distribution of estimated median PGA levels according to Akkar et al. (2014).

inspected buildings closer to the SAMA are identified less than DG2 (**Supplementary Figure S2**). The spectral accelerations of SMG1 and SAMA are compared with the EAK2003 design spectra for 5% of damping ratios. Both horizontal components of records exceed the design spectra of all soil types in EAK2003 at a time of around 0.5 s. The damage grade of the inspected buildings in Kuşadası (Turkey) are identified less than two albeit a considerable recorded PGA value as well as the exceedance of SA to all design spectra at the period of 0.5 s. The relatively lower PGAs and spectral accelerations under the design spectra are seen in the other selected stations of the Turkish side and this argument is completely consistent with the lower damage grades of the investigated buildings. It is also noteworthy to be mentioned that baseline corrections and band-pass filtering have been applied to all recorded strong ground motion time histories.

For the needs of the fragility assessment, the ground motion intensity at the location of each building needs to be determined. Peak Ground Acceleration (PGA) is used here as the intensity measure type in line with other empirical fragility studies. The PGA level at the location of each building is estimated from the ground motion prediction equation (GMPE) proposed by Akkar et al. (2014). This GMPE was deemed a good predictor for the actual PGA levels for two reasons. Firstly, it is based on a Pan-European database, which includes pre-dominantly records from Italy, Greece, and Turkey. Secondly, for distances less than 70 km, the comparisons and residual analyses showed good agreement with ground motion records from the 2020 Aegean earthquake. The adopted GMPE accounts for nonlinear site effects through the average shear wave velocity in the top 30 m of a site ($V_{s,30}$), which is available at the location of each building via the USGS topography-based $V_{s,30}$ maps (Allen and Wald, 2007). The Akkar et al. (2014) GMPE also calculates the PGA levels from the epicentral distances (up to 200 km), which are easy to determine. Earthquake source effects are also included in their equation through the use of the moment magnitude, that best reflects the earthquake's energy level, and accounting for different faulting types. The distribution of PGA levels in the affected area is depicted in **Figure 9**. It should be noted that only the best-estimate of PGA is estimated from the adopted GMPE and the uncertainty in the ground motion is ignored in line with common practice in the field.

TABLE 1 | Summary of field data for traditional buildings used for the empirical construction of fragility curves.

Database	EMS98 damage Scale						Total	PGA (in g)
	DG0	DG1	DG2	DG3	DG4	DG5		[min, max]
Greece	19	14	38	29	9	3	112	[0.14, 0.34]
Turkey	14	11	3	0	0	0	28	[0.04, 0.12]
Total							140	-

A summary of the main characteristics of the field data used in the empirical fragility assessment is depicted in **Table 1**. The range of PGA values estimated by Akkar et al. (2014) at the location of each building is also provided for the two countries. It can be seen that the majority of the observed data is from Samos and have experienced slightly higher PGA levels than their Turkish counterparts.

In what follows, the framework for the empirical fragility assessment is presented and then it is applied to the database compiled by the 2020 Aegean reconnaissance mission. As the number of buildings which sustained DG5 is very small, only four fragility curves (i.e., corresponding to DG1-DG4) are constructed for vernacular buildings, which are then compared with existing empirical fragility curves constructed for Greek vernacular buildings in the aftermath of several earthquakes.

3.2 Framework

The proposed fragility assessment methodology has three main steps. In the first step, an exploratory analysis aims to (i) assess the trends that the available data follow (ii) determine the main explanatory variables (i.e., the ground motion intensity measure or the building typology), that need to be included in the statistical model to better predict the likelihood of damage and (iii) assess their influence on the slope and intercept of the fragility curves. Based on the observations of the exploratory analysis, a statistical model is constructed and its goodness-of-fit to the data is examined.

3.2.1 Exploratory Analysis

To explore the relationship between the ground motion intensity and the probability of damage, a Generalised Linear Model (GLM) is fitted, as proposed by the GEM Guidelines (Rossetto et al., 2014) to the data. A GLM assumes that the response variable y_{ij} is assigned one if the building j sustained damage $Dg \geq DG_i$ and 0 otherwise. The variable follows a Bernoulli distribution:

$$y_{ij} \sim \ Bernoulli\left(\pi_i\left(\tilde{x}_j\right)\right) \tag{1}$$

where $\pi_i(\tilde{x}_j)$ is the probability that a building j will reach or exceed the 'true' damage state DG_i given estimated ground motion intensity level $\tilde{x}_j$. The Bernoulli distribution is characterised by its mean:

$$\mu_{ij} = \ \pi_i\left(\tilde{x}_j\right) \tag{2}$$

which is expressed here in terms of a probit model, commonly used to express the mean in the empirical fragility assessment field (Rossetto et al., 2013) defined in terms of Φ [.], the cumulative distribution function of a standard normal distribution:

$$\Phi^{-1}\left[\pi_i\left(\tilde{x}_j\right)\right] = \ \eta_{ij} \tag{3}$$

where η_{ij} is the linear predictor, which can be written in the form:

$$\eta_{ij} = \ \theta_{0i} + \ \theta_{1i} \ln\left(\tilde{x}_j\right) \tag{4}$$

where θ_{1i}, θ_{0i} are the two regression coefficients, representing the slope and the intercept, respectively, of the fragility curve corresponding to damage state DG_i. The confidence in the exact shape of the mean curves is estimated and presented in terms of the 90% confidence intervals around the best-estimate curves.

3.2.2 Fitting a Parametric Model

Based on the outcome of the exploratory analysis, parametric statistical models are constructed in order to construct fragility curves for the four damage states $i = \{1, 2, 3, 4\}$ for which there are sufficient data and to examine whether the slope of the aforementioned curves varies for each damage state.

The response variable y_{ij} of a suitable parametric statistical model is the damage state $i = \{0, 1, 2, 3, 4\}$ sustained by a building j. The damage state follows a categorical distribution (i.e., also called a generalized Bernoulli distribution) which describes the possible levels of damage $i = \{0, 1, 2, 3, 4\}$ sustained by a given building (**Table 1**). The random component of this model can be written as:

$$y_{ij} \sim Categorical\left(P\left(DG = \ DG_i|\tilde{x}_j\right)\right) \tag{5}$$

where $P(DG = \ DG_i|\tilde{x}_j)$ is the probability that a building j will reach the 'true' damage state ds_i given estimated ground motion intensity level $\tilde{x}_j$:

$$P\left(DG = \ DG_i|\tilde{x}_j\right) = \begin{cases} 1 - \ \pi_i\left(\tilde{x}_j\right), & i = 0 \\ \pi_i\left(\tilde{x}_j\right) - \ \pi_{i+1}\left(\tilde{x}_j\right), & 0 < i < i_{\max} \\ \pi_i\left(\tilde{x}_j\right), & i = i_{\max} \end{cases} \tag{6}$$

With regard to the link function, only the commonly used probit function is considered in the form:

$$\eta_{ij} = \Phi^{-1}\left[\pi_i\left(\tilde{x}_j\right)\right] \tag{7}$$

The linear predictor is finally expressed in two forms of increasing complexity, as depicted in Eq. 19:

$$\eta_{ij} = \begin{cases} \theta_{0i} + \ \theta_1\tilde{x}_j & (8.1) \\ \theta_{0i} + \ \theta_{1i}\tilde{x}_j & (8.2) \end{cases}$$

where $\theta_{0,1}$ are the unknown regression coefficients of the model. **Eq. 8** assume that the fragility curves are only influenced by the ground motion intensity type. **Eq. 8** assumes that the slope of the fragility curves is the same for all damage states. By contrast, **Eq. 8** allows the slope of each curve to vary for each damage state; the slope varies for each fragility curve. The combinations of random and systematic components result in two distinct models (**Table 2**).

The two models are fitted to the field data. Their goodness of fit is, then, examined by two formal tests, as proposed in the GEM guidelines (Rossetto et al., 2014). Firstly, we compare the Akaike Information Criterion (AIC) values (Akaike, 1974), which estimates the prediction error of the examined models. The model with the lowest value fits the data best. The confidence intervals for the model which fits the data best are obtained by bootstrap analysis. According to the latter analysis, 1,000 samples of the database are obtained with replacement and the model is refitted to each sample.

3.3 Construction of Fragility Curves

The framework presented in **Section 3** is adopted here in order to empirically construct the fragility curves for the traditional buildings. As part of the exploratory analysis, a GLM probit model is fitted to the data and the results are depicted in **Figure 10**. By comparing the best-estimate fragility curves, it can be noted that the likelihood of damage increases with the increase in the PGA level for all damage states. Apart from the intercept, the slope also appears to vary for the various damage

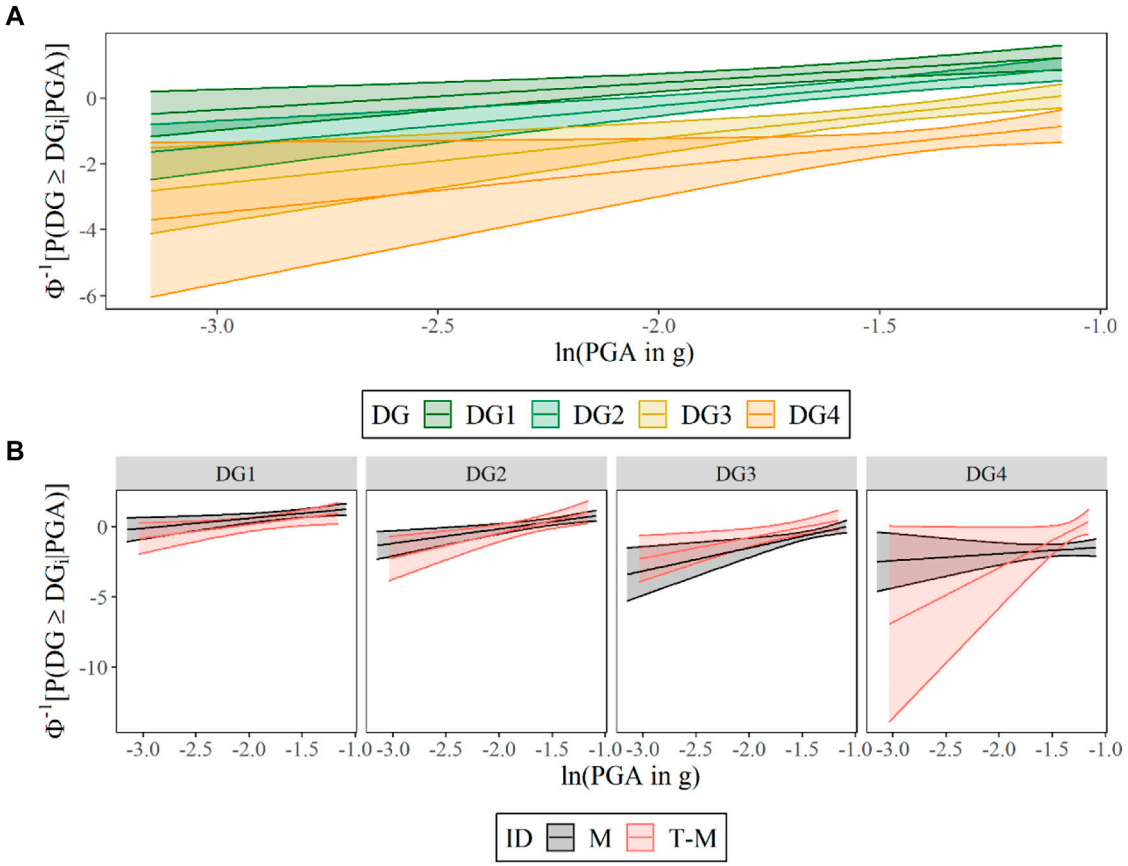

FIGURE 10 | Best-estimate fragility curves and their 90% confidence intervals corresponding to four damage states obtained by fitting probit models to **(A)** all data in the database irrespective of building typology and **(B)** subsets of data, i.e., masonry and hybrid timber-masonry buildings to assess the impact of building typology to the slope and intercept of the curves.

states, indicating the need to take this into account to the final model. With regard to the uncertainty expressed in terms of the 90% confidence intervals around the best-estimate fragility curves, the uncertainty appears to be reasonably well-constrained around each damage state with the exception of DG4. The partial overlapping of the confidence intervals can be mainly attributed to the small sample size and part of it could be attributed to the uncertain seismic behavior of vulnerable masonry buildings which are the majority of the buildings in the database. For this damage state, the uncertainty is notable and can be attributed to the very few buildings which sustained heavy damage or were destroyed.

A probit model is also fitted to subsets of data in order to construct curves for masonry and hybrid timber-masonry buildings. In **Figure 10B**, it can be noted that the fragility curves for the latter building class have very large confidence intervals which include substantially the ones for masonry buildings for all four damage states. The rather wide intervals can be attributed to the very small sample size for the hybrid buildings, and for this reason, there is not enough information to draw meaningful conclusions on whether the hybrid timber-masonry buildings behaved better than their masonry counterparts. For this reason, the final statistical model considers only the masonry buildings.

TABLE 2 | Statistical models examined here, their AIC value and the *p*-value of the log-likelihood test.

Model	Component		AIC	Likelihood Ratio Test (*p*-value)
	Random	Systematic		
M1	Eq. 1	Eq. 8.1	312.05	0.09
M2		Eq. 8.2	311.48	

Based on the observations of the exploratory analysis, the statistical model M2 (see **Table 2**) is suitable as it assumes that the only the ground motion intensity affects the likelihood of damage and allows for both the intercept as well as the slope of the fragility curves to change with each damage state. A simpler model M1 is also constructed and fitted to the data in order to compare it with the model M2 and identify which presents the best fit to the data. In **Table 2**, the comparison of the AIC values shows that model M2 fits closest to the data. Nonetheless, the differences in the AIC value is rather small.

It can be noted that the model M2 is nested to M1, which means that the more complex model includes all the terms of the simpler one plus an additional term. For this reason, a likelihood

TABLE 3 | Best estimate and standard error of the two regression coefficients for the fitted parametric model.

Name	θ_{0i}		θ_{1i}	
DG	**Best estimate**	**Standard Error**	**Best estimate**	**Standard Error**
DG1	2.57	0.363	1.07	0.201
DG2	1.99	0.347		
DG3	1.12	0.328		
DG4	0.06	0.338		

TABLE 4 | Key characteristics of the existing fragility curves used in this study.

ID	Type	Event	Reference	Building class			Damage Scale	PGA Estimation	PGA Estimation Reference
				Material / Structural system	Construction Date	Height			
M	Function	2003 Lefkada	Karababa and Pomonis (2011)	Stone masonry with flexible timber diaphragms	1919 <	Low-Rise	EMS98	PSI to PGA	Spence et al. (1991)
M	Function	2003 Lefkada	Karababa and Pomonis (2011)	Stone masonry with flexible timber diaphragms	1919 ≤ & ≤ 1945	Low-Rise	EMS98	PSI to PGA	Spence et al. (1991)
M	Function	2003 Lefkada	Karababa and Pomonis (2011)	Stone masonry with flexible timber diaphragms	1946 ≤ & ≤ 1960	Low-Rise	EMS98	PSI to PGA	Spence et al. (1991)
M	Function	2003 Lefkada	Karababa and Pomonis (2011)	Stone masonry with flexible timber diaphragms	1961 ≤	Low-Rise	EMS98	PSI to PGA	Spence et al. (1991)
T-M	Function	2003 Lefkada	Karababa and Pomonis (2011)	Dual load-bearing stone masonry and timber frame	≤ 1945	Low-Rise	EMS98	PSI to PGA	Spence et al. (1991)
M	Data	2003 Lefkada	Karababa and Pomonis (2011)	Stone masonry with timber floors	Mostly ≤ 1960	Low-Rise	EMS98	GMPE	Akkar et al. (2014)
M	Function	1993 Pyrgos 1995 Aegion 2003 Lefkada	Kassaras et al. (2020)	Stone masonry	≤ 1960	Low-Rise	EMS98	EMS98 to PGA	Tselentis and Danciu (2008)
M	Function	2003 and 2015 Lefkada	Pomonis et al., 2014	Masonry with flexible timber diaphragms	Mostly ≤ 1960	Low-Rise	EMS98	EMS98 to PGA	Tselentis and Danciu (2008)
M	Data	2015 Lefkada	Pomonis et al., 2014	Masonry with flexible timber diaphragms	Mostly ≤ 1960	Low-Rise	EMS98	GMPE	Akkar et al. (2014)

ratio test is also performed to test the null hypothesis that the two models (i.e. M1 and M2) fit equally well the data. In **Table 2**, the *p*-value of the test is found to be equal to 0.09 which means that the fit of the more complex model M2 is not statistically significant. Thus, the simpler model M1, which assumes identical slope for each fragility curve, provides the best fit to the field data.

Having established that model M2 fits the data best, the best-estimate and standard error of its regression coefficients obtained are depicted in **Table 3**.

3.4 Comparison With Existing Fragility Curves

A comparison of the constructed and existing empirical fragility curves is presented here. A search of the literature, focused on empirical fragility curves for traditional buildings in the two countries of interest, identified only three studies for Greek traditional buildings and none for their Turkish counterparts. Two of these studies used data from more than one earthquake to construct their fragility curves. Interestingly, the large database from the 2003 Lefkada earthquake has been used to construct the curves for all three studies (**Table 4**).

As part of their fragility assessment, all three existing studies expressed the fragility curves in terms of macroseismic intensity measures. Thus, to make them comparable with the curves produced in this study, their macroseismic intensity was transformed to PGA using appropriate equations found in the literature (Spense et al., 1991; Tselentis and Danciu, 2008). The fragility curves in terms of PGA are plotted in **Figure 11**. The comparison of the curves based exclusively from data from the 2003 Lefkada event (Karababa and Pomonis, 2011), shows that the curves for the hybrid timber-masonry buildings behave approximately the same as good quality masonry buildings and this further reinforces the approach adopted in this study which constructed fragility curves for traditional building and did not exclude the hybrid timber-masonry ones. It can also be noted that the curves based on the 2020 Aegean reconnaissance mission data compare well with these curves. Furthermore, the masonry buildings based on (Karababa and Pomonis, 2011) appear, in **Figure 11**, to be more vulnerable than the masonry buildings based on data from the 2003 as well as the 2015 Lefkada earthquakes (Kassaras et al., 2020). This is in line with findings by Kassaras et al. (2020) and can be attributed to the large number of retrofitted masonry buildings in the aftermath of the 2003 event. Interestingly, the curves (Pomonis et al., 2014) constructed for three Greek events (i.e., dominated by the data from the 2003 Lefkada event) also appear to be flatter and shifted to the right than the curves developed by Karababa and Pomonis

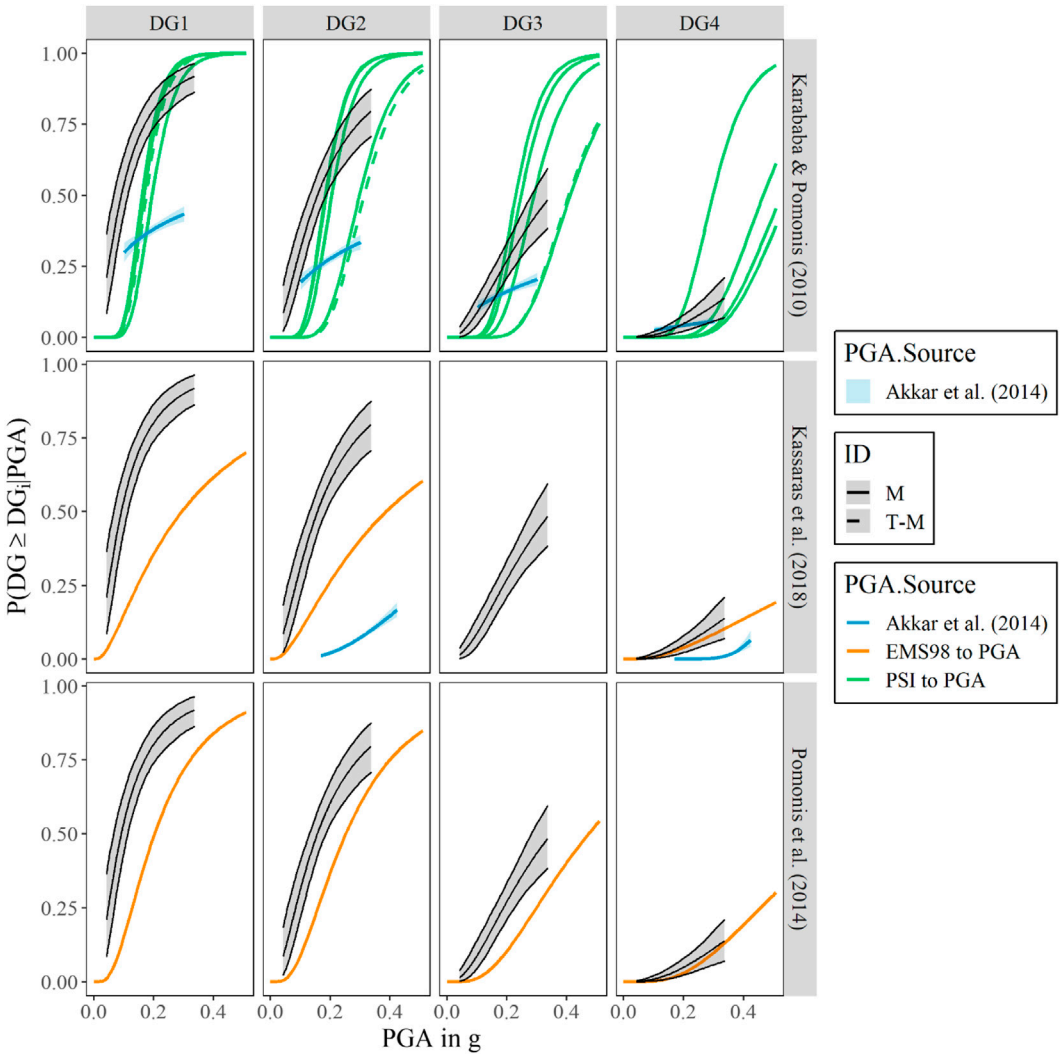

FIGURE 11 | Comparison of fragility curves constructed here (in black thicker lines) with existing fragility curves.

(2011) (as well as the curves constructed in this study). The significance of this difference is difficult to assess without the presence of confidence intervals. It could be attributed to the sensitivity of the results to the transformation from one ground motion intensity measure to another, which is associate with considerable uncertainty. The differences in the shape of the fragility curves raises questions regarding the reliability of the transformed curves in terms of PGA.

To address this challenge, the post-disaster data found in Karababa and Pomonis (2011) and kindly provided by the authors of Kassaras et al. (2020), for masonry buildings are fitted a probit model as described in Section 4.1.2 allowing for the slope of the fragility curves to vary with the damage grade. It should be mentioned that the overall database includes data from 4,800 buildings aggregated at municipality level. The database includes both buildings surveyed by the authorities as well as the census buildings used to estimate the total number of undamaged buildings for each municipality. For these analyses, the ground motion intensity at the administrative centre of each municipality is expressed in terms of PGA, estimated by Akkar et al. (2014) GMPE to make them directly comparable to the curves constructed as part of this study. In **Figure 11**, the obtained curves are compared with the fragility curves based on the 2020 Aegean reconnaissance mission data. When compared to the curves based on the 2015 Lefkada data, for all damage states the masonry buildings affected by the 2020 Aegean earthquake clearly appear to be more vulnerable than their counterparts in Lefkada, which is expected given the large number of retrofitted buildings noted during the field surveys. The curves based on data from the 2003 Lefkada event also appear to be flatter and shifted to the right from their counterparts estimated by the same data but based on a transformed intensity measure. This significant difference highlights the sensitivity in the intensity level estimation approach. When compared to the curves based on the 2020 Aegean reconnaissance mission data, it can be seen that the masonry buildings surveyed in the mission

appear to be more vulnerable than the masonry buildings in Lefkada for all damage states apart from the most severe damage (i.e., DG4). This notable discrepancy can be attributed to the limited number of buildings surveyed in the field and highlights the key role of extensive field work required for the construction of reliable fragility curves from reconnaissance missions.

4 DISCUSSION AND CONCLUSIONS

This study summarises the findings from the fieldwork of the EEFIT Mission to 30th October 2020 Aegean Earthquake with specific emphasis on joint traditional building typologies of Turkey and Greece. While disaster reconnaissance studies do often focus on the performance of heritage structures, this is commonly limited to monumental structures, and traditional/vernacular typologies are commonly overlooked. This study aimed to detail the performance of these unique building stocks through a thorough fieldwork to delineate the damage levels and mechanisms. Key limitations of this study are the limited number of buildings surveyed in the field and that all buildings were surveyed externally from the street, which might have caused an underestimation of the damage in certain cases. Another critical issue especially pertinent to the damage assessment of traditional structures that are often aged and infrequently well-maintained is to differentiate the pre-existing damage. While in this study this barrier was tried to be overcome with a careful appraisal of the damage and regular reference to street view images, it is possible that some damage was wrongly (un)assigned to the seismic event under question.

One of the examined traditional building typologies of the Aegean region is the hybrid timber-masonry constructions, which are also common in the rest of Greece and Turkey, as well as most of the Balkans. The previous experimental and analytical work (Aktas et al., 2014; Aktas and Turer, 2016) suggest that the construction technology adopted for the timber framing for these structures is beneficial under earthquake loading owed to high ductility of nailed connections, high lateral load bearing capacity thanks to braced timber frames, and low seismic mass of these structures, especially when cladded rather than infilled, although there are certain prerequisites for an overall desirable performance, including the performance of the masonry ground floor and good connections between various structural components. Our field observations and data collected from a small set of timber-masonry structures suggest that these advantageous technological characteristics were partly overcome by accumulated material and structural damage due to not being in use or being poorly maintained, which is especially critical for the timber components and connections, and also compromises the strength of masonry walls and connections. The typical failure mode for timber-masonry structures is primarily, and in line with the existing literature, failure of masonry. While this is commonly limited to stonework infill of the timber framed upper storeys, when this happens on the ground floor it may compromise the structural stability of the entire building, leading to progressive collapse. The analyses presented in this paper show that the expected structural performance of timber-masonry buildings is largely comparable to that of the masonry buildings surveyed in this study for low-to moderate-damage levels, although we did not have a large enough dataset to drive more robust conclusions on this. For traditional masonry structures, out-of-plane failure mode is observed but is limited to higher elevations of the facades, or to corner failure, while in-plane failure in piers and spandrels is more common. Poorly connected multi-leaf masonry seems to be widespread, as is revealed by these failures. For these buildings, too, the poor state of conservation is critical, affecting especially floor and roof systems. Fragility analyses carried out for the surveyed masonry structures on the other hand showed that, assuming our sample set reflects well the characteristics of the building stock as a whole, the expected vulnerability for the Aegean masonry building stock was higher than the Lefkada stock.

DATA AVAILABILITY STATEMENT

The datasets presented in this article are not readily available because of ongoing work, however can be made available at an aggregated level upon reasonable request. Requests to access the datasets should be directed to YA, y.aktas@ucl.ac.uk.

AUTHOR CONTRIBUTIONS

Conceptualisation YA and II; Data Analysis YA, II, AV, MK, DK-F, JB, and BD; Data Collection PD; Funding YA; Manuscript preparation YA, II, FM, FD-A, and KD.

FUNDING

This study was carried out as an extension to the EEFIT Mission to 30 October 2020 Aegean Earthquake and Tsunami, and the authors are grateful to EEFIT and the EPSRC-funded Learning from Earthquake (LfE) Building Resilient Communities Through Earthquake Reconnaissance, Response and Recovery (EP/P025641/1) for supporting this activity.

ACKNOWLEDGMENTS

We cordially thank to our field crews in Turkey and Greece. We are also indebted to the communities in the affected areas for their help and support during the data collection. All pictures are EEFIT Aegean Mission Team's, unless otherwise stated. The support of the UCL Open Access for the open access publication fees is also gratefully acknowledged.

SUPPLEMENTARY MATERIAL

The Supplementary Material for this article can be found online at: https://www.frontiersin.org/articles/10.3389/fbuil.2022.840159/full#supplementary-material

REFERENCES

Akaike, H. (1974). A New Look at the Statistical Model Identification. *IEEE Trans. Automat. Contr.* 19 (6), 716–723. doi:10.1109/tac.1974.1100705

Akkar, S., Sandıkkaya, M. A., and Bommer, J. J. (2014). Empirical Ground-Motion Models for point- and Extended-Source Crustal Earthquake Scenarios in Europe and the Middle East. *Bull. Earthquake Eng.* 12 (1), 359–387. doi:10.1007/s10518-013-9461-4

Aktas, Y. D., Akyuz, U., Turer, A., Erdil, B., and Sahin Guchan, N. (2014). Seismic Resistance Evaluation of Traditional Ottoman Timber-Frame Hımış Houses: Frame Loadings and Material Tests. *Earthquake Spectra* 30 (4), 1711–1732.

Aktas, Y. D., Ioannou, I., Malcioglu, F. S., Kontoe, M., Parammal Vatteri, A., Durmaz, B., et al. (2022). "Hybrid Earthquake Reconnaissance Mission to 30 October 2020 Aegean Sea Earthquake and Tsunami(Izmir, Turkey & Samos, Greece): Description of Data Collection Methods and Damage," in *Frontiers in Built Environment: Earthquake Engineering*. doi:10.3389/fbuil.2022.840192

Aktas, Y. D., O'Kane, A., Ozden, A. T., Parammal Vatteri, A., Durmaz, B., Kazantzidou-Firtinidou, D., et al. (2021). *The Aegean Earthquake and Tsunami of 30 October 2020*. London: EEFIT.

Aktas, Y. D. (2017). Seismic Resistance of Traditional Timber-Frame Hımış Structures in Turkey: a Brief Overview. *Int. Wood Prod. J.* 8 (Suppl. 1), 21–28.

Aktas, Y. D., and Turer, A. (2016). Seismic Performance Evaluation of Traditional Timber Hımış Frames: Capacity Spectrum Method Based Assessment. *Bull. Earthquake Eng.* 14 (11), 3175–3194.

Allen, T. I., and Wald, D. J. (2007). Topographic Slope as a Proxy for Seismic Site-Conditions (VS30) and Amplification Around the globe. *Geol. Surv. (Us)*. doi:10.3133/ofr20071357

Ambraseys, N. N., and Jackson, J. A. (1981). Earthquake hazard and Vulnerability in the Northeastern Mediterranean: the Corinth Earthquake Sequence of February-March 1981. *Disasters* 5 (4), 355–368. doi:10.1111/j.1467-7717.1981.tb01108.x

Ambraseys, N. N., and Zatopek, A. (1969). The Mudurnu Valley, West Anatolia, Turkey, Earthquake of 22 July 1967. *Bull. Seismological Soc. America* 59 (2), 521–589. doi:10.1785/bssa0590020521

Biricik, A. S., Ceylan, M. A., and Ünlü, M. (1996). Ekim 1995-Dinar Depremi. *Marmara Coğrafya Dergisi* 1 (1), 63–102.

Boore, D. M., Stewart, J. P., Skarlatoudis, A. A., Seyhan, E., Margaris, B., Theodoulidis, N., et al. (2021). A Ground-Motion Prediction Model for Shallow Crustal Earthquakes in Greece. *Bull. Seismological Soc. America* 111 (2), 857–874. doi:10.1785/0120200270

D'Ayala, D., and Paganoni, S. (2011). Assessment and Analysis of Damage in L'Aquila Historic City centre after 6th April 2009. *Bull. Earthquake Eng.*, 81–104.

Diri, F. (2010). *Construction Techniques of Traditional Birgi Houses*. Ankara: Middle East Technical UniversityMsc Thesis.

Dutu, A., Niste, M., Spatarelu, I., Dima, D. I., and Kishiki, S. (2018). Seismic Evaluation of Romanian Traditional Buildings with Timber Frame and Mud Masonry Infills by In-Plane Static Cyclic Tests. *Eng. Structures* 167, 655–670. doi:10.1016/j.engstruct.2018.02.062

EAK (2003). *Greek Seismic Code*. Athens–Greece: Earthquake planning & protection organization. (in Greek).

EN (2004). *Eurocode 8: Design of Structures for Earthquake Resistance - Part 1: General Rules, Seismic Actions and Rules for Buildings, European Standard EN 1998-1:2004*. Brussels, Belgium: European Committee for Standardisation.

Erdik, M., Demircioglu, M., Beyen, K., Sesetyan, K., Aydinoglu, N., Gul, M., et al. (2003). May 01, 2003 Bingol (Turkey) Earthquake. EERI. Available at: https://www.eeri.org/lfe/pdf/turkey_bingol_reconnaissance_report_erdik.pdf (Accessed August 08, 2021).

Erdik, M., Sestyan, K., Demircioglu, M. B., Biro, Y., and Uckan, E. (2002). Preliminary Observations on the Sultandagi, Turkey, Earthquake of February 3, 2002. EERI. Available at: https://www.eeri.org/lfe/pdf/Turkey_Sultandagi_Insert_May02.pdf (Accessed August 08, 2021).

Erdik, M., Yüzügüllü, Ö., Yilmaz, C., and Akkas, N. (1992). 13 March, 1992 (Ms=6·8) Erzincan Earthquake: A Preliminary Reconnaissance Report. *Soil Dyn. Earthquake Eng.* 11, 279–310. doi:10.1016/0267-7261(92)90044-e

Gocer, C. (2020). Field Investigation of the Performance of Unreinforced Masonry Building Structures during the June 12, 2017, Lesvos Earthquake in the Aegean Sea. *J. Perform. Constructed Facil.* 34 (5). doi:10.1061/(asce)cf.1943-5509.0001497

Gülhan, D., and Özyörük Güney, İ. (2000). "The Behaviour of Traditional Building Systems against Earthquake and its Comparison to Reinforced Concrete Frame Systems," in *Experiences of Marmara Earthquake Damage Assessment Studies in Kocaeli and Sakarya* (Istanbul: ICOMOS).

Karababa, F. S., and Pomonis, A. (2011). Damage Data Analysis and Vulnerability Estimation Following the August 14, 2003 Lefkada Island, Greece, Earthquake. *Bull. Earthquake Eng.* 9 (4), 1015–1046. doi:10.1007/s10518-010-9231-5

Karantoni, F. V., and Bouckovalas, G. (1997). Description and Analysis of Building Damage Due to Pyrgos, Greece Earthquake. *Soil Dyn. Earthquake Eng.* 16, 141–150. doi:10.1016/s0267-7261(96)00035-8

Kassaras, I., Kazantzidou-Firtinidou, D., Ganas, A., Tonna, S., Pomonis, A., Karakostas, C., et al. (2020). On the Lefkas (Ionian Sea) November 17, 2015 Mw=6.5 Earthquake Macroseismic Effects. *J. Earthquake Eng.* 24 (12), 1913–1943. doi:10.1080/13632469.2018.1488776

Malcioglu, F. S., O'Kane, A., Dönmez, K., and Aktaş, Y. D. (2022). "Characteristics of Strong Ground Motions in the 30 October 2020, MW6.9 Aegean Sea Earthquake," in *Frontiers in Built Environment: Earthquake Engineering*. doi:10.3389/fbuil.2022.870279

Mikres Diadromes Samou (2020). *Mikres Diadromes Samou*. Retrieved from Youtube: https://www.youtube.com/channel/UC2eraxpvAND7VFC6F7GEqGw.

Noore, D. M., Stewart, J. P., Skarlatoudis, A. A., Seyhan, E., Margaris, B., Theodoulidis, N., et al. (2021). A Ground-motion Prediction Model for Shallow Crustal Earthquakes in Greece. *Bull. Seismological Soc. America* 111 (2), 857–874.

Papaioannou, K. (1961). *Samos: Traditional Greek Architecture*. Melissa.

Pitilakis, K., Gazepis, C., Anastasiadis, A., and Vancouver, B. C. (2004). *Design Response Spectra and Soil Classification for Seismic Code Provisions. 13th World Conference on Earthquake Engineering*. Canada, August 1-6, 2004Paper No. 2904.

Pomonis, A., Gaspari, M., and Karababa, F. (2014). Seismic Vulnerability Assessment for Buildings in Greece Based on Observed Damage Data Sets. *Bollettino di Geofisica Teorica Ed. Applicata* 55 (2), 501–534.

Rossetto, T., Ioannou, I., and Grant, D. N. (2013). *Existing Empirical Fragility and Vulnerability Functions: Compendium and Guide for Selection*. Pavia, Italy: GEM Foundation.

Rossetto, T., Ioannou, I., Grant, D. N., and Maqsood, T. (2014). *Guidelines for the Empirical Vulnerability Assessment*. Pavia, Italy: GEM Foundation.

Sahin Guchan, N. (2018). History and Characteristics of Construction Techniques Used in Traditional Timber Ottoman Houses. *Int. J. Architectural Heritage* 12 (1). doi:10.1080/15583058.2017.1336811

Spense, R. J., Coburn, A. W., Sakai, S., and Pomonis, A. (1991). "A Parameterless Scale of Seismic Intensity for Use in Seismic Risk Analysis and Vulnerability Assessment," in *SECED,* Earthquake, Blast And Impact (Elsevier), 19–30.

Tselentis, G.-A., and Danciu, L. (2008). Empirical Relationships between Modified Mercalli Intensity and Engineering Ground-Motion Parameters in Greece. *Bull. Seismological Soc. America* 98 (4), 1863–1875. doi:10.1785/0120070172

Vintzileou, E., Zagkotsis, A., Repapis, C., and Zeris, C. (2007). Seismic Behaviour of the Historical Structural System of the Island of Lefkada, Greece. *Construction Building Mater.* 21 (1), 225–236. doi:10.1016/j.conbuildmat.2005.04.002

Vlachakis, G., Vlachaki, E., and Lourenço, P. B. (2020). Learning from Failure: Damage and Failure of Masonry Structures, after the 2017 Lesvos Earthquake (Greece). *Eng. Fail. Anal.* 117, 104803. doi:10.1016/j.engfailanal.2020.104803

Williams, M. S., Pomonis, A., Booth, E. D., Vaciago, G., and Ring, S. (1992). The Erzincan, Turkey Earthquake of 13 March 1992. EEFIT. Available at: https://www.istructe.org/IStructE/media/Public/Resources/report-eefit-erzincan-turkey-20190812.pdf (Accessed August 08, 2021).

Conflict of Interest: The authors declare that the research was conducted in the absence of any commercial or financial relationships that could be construed as a potential conflict of interest.